A Packet-Level Model for UWB Channel with People Shadowing Process Based on Angular Spectrum Analysis

Ruonan Zhang and Lin Cai, *Member, IEEE*

Abstract—**Ultra-wideband (UWB) wireless communication technologies have been proposed to support high data rate multimedia services in office or residential environments. Due to the low transmission power of UWB, the shadowing effect by moving people can considerably reduce the received signal quality and thus significantly degrade the quality of service (QoS) of on-going transmissions. An open issue is to build a simple model which captures the temporal variation of UWB channels and the packet error rate (PER) due to the people shadowing effect (PSE), which will be a useful tool for upper layer protocol performance analysis and simulation. This paper presents an analytical study of the PSE and the temporal variation of UWB channels induced by the motion of a person. First, we derive the angular power spectral density (APSD) of the indoor UWB channel impulse response (CIR), and the PSE in terms of signal power attenuation. Second, based on a two-dimensional random walk mobility model, the PER variation due to people shadowing is modeled as a finite-state Markov chain (FSMC). The investigation of APSD provides important insights on the spatial propagation characteristics of UWB signals. The proposed packet-level channel model can be conveniently incorporated into analytical frameworks and simulation tools for evaluating upper-layer protocols of UWB networks.**

Index Terms—**Channel model, UWB, angular power spectral density, shadowing effect.**

I. INTRODUCTION

ULTRA-WIDEBAND (UWB) is an appealing technology for short-range, high data-rate wireless communications [1]. It is well suited for wireless personal area networks (WPANs) in office or residential buildings to support multimedia services. In such intensive multipath propagation environments, the range and robustness of UWB communications depend on efficient energy collection from significant paths. However, people moving in the proximity of the transceivers may frequently penetrate and shadow the significant paths, like the line-of-sight (LOS). Measurements of the signal propagation of a fixed UWB link in [2]–[6] have revealed that the people shadowing effect (PSE) can induce the attenuation on the received signal power by up to 8 dB if both transceivers

employ omni antennas or 15 dB with directional antennas. Furthermore, the random motion of people can cause significant fluctuations of the received signal-to-noise ratio (SNR) and even totally interrupt the data transfer. Therefore, the PSE and UWB channel fading should be considered properly in the design and evaluation of UWB systems and network protocols. For example, the channel estimation techniques depend on the temporal correlations of the channel impulse response (CIR). The channel fading can increase considerably the packet loss rate and queuing/transmission delay, which eventually affect the user's perceived quality of service (QoS).

In the literature, the impact of moving people on a fixed UWB link has been measured extensively. Reference [2] and [3] illustrated the received power attenuation by one or several persons in a corridor or a square conference room, respectively. In [4] and [5], the PSE was measured when a person moved along a line perpendicular to the LOS and fully or partially blocked the LOS. In [6], Ghaddar *et. al.* conducted the continuous wave measurements with the presence of an obstacle (a person or a metallic cylinder) moving parallel to or perpendicularly crossing the LOS. These measurements have revealed the following key observations. First, the shadowing effect (power attenuation) depends on the position of the obstacle, especially its angular location and distance from the antennas. Second, if the persons are moving outside the proximity of UWB transceivers (*i.e.*, not obstructing the significant paths), the CIR and the received power do not have substantial variation.

Although substantial modeling efforts have been done for the large- and small-scale fading of the indoor UWB channels [7] (and the references therein), the PSE has not been investigated or modeled theoretically. In addition, the physical layer channel models are too complex to be used for network protocol analysis and simulations, which makes the optimization of upper-layer protocols considering realistic propagation environments virtually impossible and hampers the research in this promising area. In [8], simulations were used to estimate the angular power spectral density (APSD) to describe the shadowing process and develop a simple channel model (assuming a person moving along a straight line). In this paper, we obtain the APSD analytically, so we can build a general packet-level model for UWB channel with people shadowing process.

The main contributions of this paper are two-fold. First, we derive the APSD of the UWB CIR in closed-form and then

obtain the approximation of the shadowing effect analytically. Second, based on the two-dimensional random walk mobility model, we build a packet-level channel model using a finite state Markov chain (FSMC) for the time-varying shadowed channel. The proposed model can help to optimize the UWB system parameters related to temporal fading, such as channel estimation and power control. Furthermore, the model directly presents the stochastic process of the PER and hence the performance (link throughput, delay, *etc.*) of WPANs can be studied analytically considering the realistic channel characteristics. It also can be easily incorporated into network simulators like NS-2 or GloMoSim.

The remainder of the paper is organized as follows. In Section II, the average APSD of UWB channels is derived based on the IEEE 802.15.3a channel model (called 3a model in the following). In Section III, the shadowing effect of a human body is investigated, and the performance of multiband-orthogonal frequency-division multiplexing (MB-OFDM) UWB systems is studied in Section IV. The continuous-time Markov model for the time-varying UWB channels is proposed in Section V. Numerical results are given in Section VI, followed by the concluding remarks and further research issues in Section VII.

II. THE ANGULAR POWER SPECTRAL DENSITY OF UWB SIGNALS

Shadowing on a UWB channel occurs when a certain range of angle-of-arrival (AOA) of the signal is obstructed by an obstacle. Thus, the remaining received power or the PSE (in terms of power attenuation) can be estimated based on the angular distribution of the incident power and the AOAs which are blocked. The angular power spectral density (APSD) refers to the power density received at a certain azimuth θ, giving the distribution of power versus the AOA. In [9] and [10], the measurements of the spatial propagation of indoor UWB channels have shown that the AOAs of the incident rays[1] are also clustered (like the time-of-arrival characteristics) and the arrivals of rays within a cluster have a Laplacian distribution. However, analytical study of the UWB channel APSD and the PSE has not been reported in the literature. In this section, we derive the APSD in closed-form based on the standard 3a model and develop a simple modified Laplacian distribution to approximate the APSD. Our analytical results will be compared with the measurements in [9] and [10].

A. 3a UWB Channel Model

The CIR defined in the 3a model [7] is a stochastic process, composed of a series of delayed and attenuated multipath components:

$$h(t) = X \sum_{l=0}^{\infty} \sum_{k=1}^{\infty} a_{k,l} \delta(t - T_l - t_{k,l}), \qquad (1)$$

where the cluster arrivals and ray arrivals within each cluster are modeled as Poisson processes with arrival rate of Λ and $\lambda(\lambda > \Lambda)$, respectively. By definition, the delay of the first

---

[1]A ray refers to a single propagation path and corresponds to a multipath component in the continuous-time CIR in the 3a model.

cluster is $T_0 = 0$ and the arrival time of other clusters, T_l, has the distribution of $Gamma(l, \Lambda), l = 1, 2, \cdots$. The ray arrival time within a cluster, $t_{k,l}$, has the distribution of $Gamma(k, \lambda), k = 1, 2, \cdots$. The total excess delay of the k-th ray in the l-th cluster is $\tau_{k,l} = T_l + t_{k,l}$. X represents the log-normal attenuation with zero mean and variance of σ_X^2.

The multipath gain coefficients $a_{k,l}$ are modeled as: $20\log_{10}(|a_{k,l}|) \sim N(\mu_{k,l}, \sigma_1^2 + \sigma_2^2)$. The average power delay profile, $E[|a_{k,l}|^2]$, exhibits double exponential decay:

$$\Omega_{k,l} = E[|a_{k,l}|^2] = \Omega_0 e^{-T_l/\Gamma} e^{-t_{k,l}/\gamma}, \qquad (2)$$

where Ω_0 is the mean energy of the first path of the first cluster. The total energy of the multipath components is normalized such that $\Sigma_{l=0}^{\infty} \Sigma_{k=1}^{\infty} |a_{k,l}|^2 = 1$.

The constant parameters $(\Lambda, \lambda, \Gamma, \gamma, \sigma_1, \sigma_2, \text{ and } \sigma_X)$ are defined in the 3a standard [7] for four propagation scenarios (CM1~CM4). The parameters of CM1 are used throughout this work because it is the scenario with the LOS existing between the UWB transceivers.

Notice that X in (1) gives a random power attenuation to each CIR realization. As defined in the 3a model, X represents the log-normal shadowing for the purpose of comparing the performance of alternative UWB PHY systems. However, such definition does not present the realistic shadowing process in indoor environments, especially the PSE. Our work provides a suitable way to determine the shadowing term X instead of using an independent log-normal distributed random variable and reveals not only the distribution of the power attenuation but also the higher-order statistics of the channel variation (like the time-correlation property).

B. AOA Distribution and Power Density of the Rays

The AOA of each ray in the CIR is a random variable, depending on the propagation environments and the movement of scatters. The measurements in [9] and [10] have both demonstrated that the arrival azimuths of the rays are clustered and the strongest cluster is almost always concentrated in the LOS direction while the other clusters are uniformly distributed over $[-\pi, \pi)$. The rays of the strongest angular cluster, arriving at the receiver within a limited angular range in the LOS direction, have small excess delay and large energy magnitude due to relatively short propagation paths and less reflections. On the other hand, the rays of the other small angular clusters are uniformly distributed over $[-\pi, \pi)$. Their large AOA is related to more reflections and scattering, resulting in large excess delay and small energy magnitude. Therefore, the AOA of a ray can be modeled as being uniformly distributed over a certain angular spread which depends on the excess delay [11]. The probability density function (PDF) of the incident angle with respect to the LOS, θ, is:

$$f_\theta(x|\tau) = \begin{cases} \frac{\tau_m}{2\pi\tau} \text{rect}\left(\frac{\tau_m}{2\pi\tau}x\right), & 0 < \tau \leq \tau_m, \ -\pi \leq x < \pi \\ \frac{1}{2\pi}, & \tau > \tau_m, \ -\pi \leq x < \pi \end{cases} \qquad (3)$$

where τ is the total delay of the ray, and $\text{rect}(\cdot)$ is the rectangular function. The parameter τ_m should be chosen such that the variance of the APSD is consistent with realistic measurements. From (3), the angular spread of the k-th ray in

$$\overline{P_{k,l}} = E[P_{k,l}|\tau_{k,l}] = \begin{cases} E\left[\frac{|a_{k,0}|^2}{t_{k,0}}\frac{\tau_m}{2\pi}\right] = \frac{\tau_m\Omega_0}{2\pi}\frac{1}{t_{k,0}}e^{-\frac{t_{k,0}}{\gamma}}, & l = 0, \ 0 < t_{k,0} \leq \tau_m \\ E\left[\frac{|a_{k,0}|^2}{2\pi}\right] = \frac{\Omega_0}{2\pi}e^{-\frac{t_{k,0}}{\gamma}}, & l = 0, \ t_{k,0} > \tau_m \\ E\left[\frac{|a_{k,l}|^2}{2\pi}\right] = \frac{\Omega_0}{2\pi}e^{-\frac{T_l}{\Gamma}}e^{-\frac{t_{k,l}}{\gamma}}, & l \geq 1. \end{cases} \tag{5}$$

the l-th cluster is $[-\phi_{k,l}/2, \phi_{k,l}/2]$, where

$$\phi_{k,l} = \begin{cases} \frac{t_{k,0}}{\tau_m}2\pi, & l = 0, \ 0 \leq t_{k,0} \leq \tau_m \\ 2\pi, & l = 0, \ t_{k,0} > \tau_m \\ 2\pi, & l \geq 1. \end{cases} \tag{4}$$

Consequently, the angular power density of the ray can be obtained as $P_{k,l} = |a_{k,l}|^2/\phi_{k,l}$. Because $|a_{k,l}|^2$ is a random variable with the mean dependent on its total delay given by (2), the average received power density conditioned on $\tau_{k,l}$ can be obtained from (2) and (4) as (5) at the top of the page. Note that because the AOA of the LOS component has no excess delay ($t_{1,0} = 0$) and no angular spread ($\phi_{1,0} = 0$), its energy should be directly added (using a Delta function) to the power density at azimuth of 0°.

C. The APSD of UWB CIR

APSD is the composite angular power distribution, *i.e.*, the total energy incident at a certain azimuth θ. Since the UWB CIR is composed of a series of delayed and attenuated rays as described in (1), the APSD at θ consists of the energy contribution from all rays whose AOA spread is larger than or equal to 2θ (*i.e.* $\theta \in [-\phi_{k,l}/2, \phi_{k,l}/2]$). The APSD of a CIR realization given the cluster delay and ray delay can be expressed as:

$$\mathbb{P}(\theta) = \underbrace{\sum_{\phi_{k,0} \geq 2|\theta|, t_{k,0} \leq \tau_m} \overline{P_{k,0}}}_{A} + \underbrace{\sum_{t_{k,0} \geq \tau_m} \overline{P_{k,0}}}_{B} + \underbrace{\sum_{l \geq 1} \overline{P_{k,l}}}_{C}, \tag{6}$$

where the summation A is the angular power density of the rays in the first cluster whose delay is less than τ_m but angular spread is larger than 2θ. Summations B and C represent the power contribution from the other rays in the first cluster and the rays in the other clusters, respectively, whose angular spread covers all angles as shown in (4).

From (4), the boundaries of the summation A can be transformed as $\frac{|\theta|}{\pi}\tau_m \leq t_{k,0} \leq \tau_m$. Because $t_{k,0}$ has the distribution of $Gamma(k, \lambda)$ as described in Section II-A, we use the expected value of $E[t_{k,0}] = k/\lambda$ as the approximation of $t_{k,0}$. Then the boundaries of the summation can be obtained as $k_0 \leq k \leq \lfloor \tau_m\lambda \rfloor$, where $k_0 = \max\{\lceil \frac{\tau_m\lambda}{\pi}|\theta| \rceil, 2\}$, because, as mentioned earlier, $k = 1$ corresponds to the LOS component and it is excluded from the summation. $\lceil \cdot \rceil$ and $\lfloor \cdot \rfloor$ are the ceiling and floor functions because k is an integer. From (5) and (6), the average APSD (excluding the LOS component) with respect to the delay terms can be obtained by (see Appendix A for derivation)

$$\overline{\mathbb{P}(\theta)} = \underbrace{\frac{\Omega_0}{2\pi}\tau_m\lambda \sum_{k_0}^{\lfloor \tau_m\lambda \rfloor} \frac{\rho^{k-1}}{k-1}}_{\bar{A}} + \underbrace{\frac{\Omega_0}{2\pi}\frac{\rho^{\lceil \tau_m\lambda \rceil}}{1-\rho}}_{\bar{B}} + \underbrace{\frac{\Omega_0}{2\pi}(\Gamma\Lambda)(\gamma\lambda)}_{\bar{C}}, \tag{7}$$

where $\rho = \frac{\lambda\gamma}{1+\lambda\gamma}$. The parameters $(\lambda, \Lambda, \gamma, \Gamma)$ are given in the 3a standard [7] or can be measured for a specific indoor environment. Ω_0 should be chosen such that the total power contained in the multipath components is normalized to one. Because $h(t)$ is a stochastic process, Ω_0 is calculated by considering the average total power of the CIR, as (see Appendix B for derivation):

$$\Omega_0 = 1/[\gamma\lambda(1 + \Gamma\Lambda)]. \tag{8}$$

From (2), Ω_0 is the energy of the 1st ray in the first cluster (LOS component) and hence should be added to the power density at 0°. From (7) and (8), the average APSD is:

$$\overline{P(\theta)} = \begin{cases} \overline{\mathbb{P}(0)} + \frac{1}{(\gamma\lambda)(1+\Gamma\Lambda)}, & \theta = 0 \\ \overline{\mathbb{P}(\theta)}, & 0 < |\theta| \leq \pi. \end{cases} \tag{9}$$

D. Comparison with Simulation and Measurements

Totally 40 CIR realizations are generated with the 3a CM1 model and the APSD of each CIR is calculated according to [11]. $\tau_m = 14$ nsec is chosen such that the standard deviation of the angular distribution is 31°, which is the average value of the measurements in [9], [10]. The averaged APSD is shown in Fig. 1. Using the parameters for CM1 [7] ($\lambda = 2.5$/nsec, $\Lambda = 0.0233$/nsec, $\gamma = 4.3$ and $\Gamma = 7.1$), the analytical result of APSD from (9) is also shown in the figure. It can be seen that the analytical estimation is quite accurate.

The measurements in [9] and [10] found that the distribution of the relative arrival angles of the rays in one cluster was best fit to the Laplacian density of $p(\theta) = \frac{1}{\sqrt{2}\sigma}e^{-\frac{\sqrt{2}}{\sigma}|\theta|}$, where the standard deviation σ varies from 25° to 37° for various environments. Because the shape of the APSD is determined by the energy distribution of the strongest angular cluster (in the LOS direction), it should be similar to a Laplacian distribution, while there is a power floor over all angles contributed from the other clusters (uniformly distributed from $-\pi$ to π). This power floor is expected because when we use omni-directional antennas in the closed spaces like the indoor environments, we should be able to received some energy over all the angles. In (7), terms $\bar{B}$ and $\bar{C}$ represent the energy contributed to all angles. Based on [9], [10], we use the modified Laplacian distribution of $p'(\theta) = \frac{1}{D}\left[\frac{1}{\sqrt{2}\sigma}\exp(-\frac{\sqrt{2}}{\sigma}|\theta|) + \bar{B} + \bar{C}\right]$ to represent the measurement results. D is used to normalize $p'(\theta)$ such that $\int_{-\pi}^{\pi} p'(\theta)d\theta = 1$. We get:

$$p'(\theta) = ae^{-\frac{\sqrt{2}}{\sigma}|\theta|} + b, -\pi < \theta \leq \pi \tag{10}$$

where $a = \frac{1}{1+2\pi(\bar{B}+\bar{C})}\frac{1}{\sqrt{2}\sigma}$ and $b = \frac{\bar{B}+\bar{C}}{1+2\pi(\bar{B}+\bar{C})}$.

The modified Laplacian distribution with $\sigma = 31^o$ is also shown in Fig. 1. Constants $\bar{B}$ and $\bar{C}$ are calculated from (7) with the parameters from the 3a CM1 model. Fig. 1 illustrates that the analytical result is close to the Laplacian distribution, which shows a good match of the analytical approximation to the realistic measurements.

$$E_r(\theta_1, \theta_2) = 1 - \int_{\theta_2}^{\theta_1} p'(\theta)d\theta = \begin{cases} 1 - \frac{a\sigma}{\sqrt{2}}(e^{-\frac{\sqrt{2}}{\sigma}\theta_2} - e^{-\frac{\sqrt{2}}{\sigma}\theta_1}) - b(\theta_1 - \theta_2), & \theta_2 \geq 0 \\ 1 - \frac{a\sigma}{\sqrt{2}}(2 - e^{-\frac{\sqrt{2}}{\sigma}\theta_1} - e^{\frac{\sqrt{2}}{\sigma}\theta_2}) - b(\theta_1 - \theta_2), & \theta_1 \geq 0, \theta_2 < 0 \\ 1 - \frac{a\sigma}{\sqrt{2}}(e^{\frac{\sqrt{2}}{\sigma}\theta_1} - e^{\frac{\sqrt{2}}{\sigma}\theta_2}) - b(\theta_1 - \theta_2), & \theta_1 < 0, \theta_2 < 0 \end{cases} \quad (11)$$
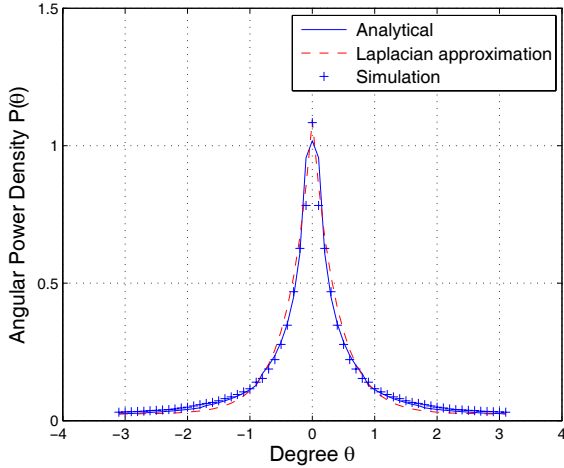

Fig. 1.   Comparison of analytical and simulation results of APSD.
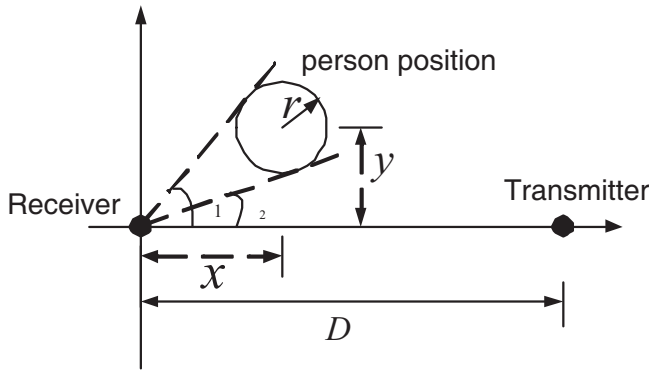
Fig. 2.   Computation of blocking angular range.

Fig. 3.   Power attenuation when a person moves along a path perpendicular to LOS.

III. PEOPLE SHADOWING EFFECT ON UWB CHANNELS

We investigate the shadowing process of the UWB channel: a single scatterer, normally a person, is moving around in the area between UWB transceivers and thus obstructing some significant paths. The body is modeled as a cylinder with radius $r = 30$ cm and obstructs a certain angular range of AOA, over which range the transmitted power cannot reach the receiver.

Let the receiver be located at the origin, the transmitter at the point $(D, 0)$ and the moving person at (x, y), as shown in Fig. 2. The obstructed angular range is $\theta_1 - \theta_2$, where $\theta_1 = \arctan(\frac{y}{x}) + \arcsin(\frac{r}{\sqrt{x^2+y^2}})$ and $\theta_2 = \arctan(\frac{y}{x}) - \arcsin(\frac{r}{\sqrt{x^2+y^2}})$. Hence, the *remaining* power of the CIR can be estimated using the APSD given in (9) or the modified Laplacian distribution in (10) for a simpler approximation. If the latter is used, the remaining received power can be obtained as (11) at the top of the page, where the total energy
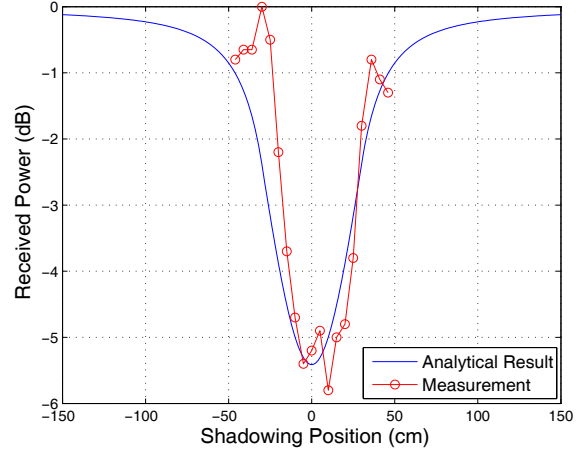
of the CIR is normalized to unity and θ_1, θ_2 depend on the person's position (x, y). The PSE, in terms of the total power attenuation (dB), is:

$$\chi(x, y) = 10\log_{10}\left[E_r(x, y)\right]. \quad (12)$$

The numerical results of PSE when a person is penetrating the LOS along a straight line from $(50, -150)$ to $(50, 150)$ (the unit is cm) is shown in Fig. 3. The measurements of such a shadowing process are given in [5], where a tank of water was used to simulate a human body and the total received energy was recorded when the obstacle was at a series of positions along the line. It can be seen that the PSE obtained by the analytical model matches the measurements reasonably well. It also illustrates that the presence of a moving person in the proximity of the receive antenna introduces severe attenuation on the received signal strength.

IV. PER ESTIMATION WITH THE PEOPLE SHADOWING EFFECT

To facilitate the simulation and analytical study of network performance, a key issue is to build a packet-level channel model which indicates the packet-error-rate (PER) directly according to the temporal variation of the channel. The performance of an MB-OFDM system [12] is investigated in this section, and the approach can be readily extended to other UWB PHY alternatives like the direct-sequence (DS)-UWB.

A. Large-scale Fading

The average SNR [2] when the distance between the UWB transceivers is D and there is no shadowing is given by the link budget as [7], [12]:

$$r(D) = P_T - L(D) - N - N_F - I, \tag{13}$$

where $P_T, L(D), N, N_F$ and I are the transmission power, path loss, thermal noise per bit, system noise figure and implementation loss, respectively. Their definitions and values can be found in [12].

As discussed in Section III, the PSE imposes attenuation on the total received power which can be regarded as large-scale fading of the indoor UWB channels (similar to the shadowing effect for narrow-band channels). the average received SNR when a person is standing at (x, y) can be obtained by (dB):

$$r'(D, x, y) = r(D) + \chi(x, y), \tag{14}$$

where $\chi(x, y)$ is from (12).

B. PER Estimation

Because of the frequency-selective fading, the instantaneous SNR and bit-error-rate (BER) of different subcarriers are random. The PER depends on both the path loss, shadowing (large-scale fading) and the time and frequency dispersion due to multipath (small-scale fading). The presence and movement of the obstacle can also cause the variation of the multipath profile. However, as shown in the system proposal [12], the PER performance of MB-OFDM on the random realizations of the CIRs are consistent and the variations in the performance are primarily due to the effect of the large-scale fading (the shadowing). This is because the MB-OFDM system has been designed to be robust against multipath, frequency-selective fading by utilizing the interleaving, channel coding, and frequency/time diversity schemes. Since the PER is mainly determined by the path loss and shadowing, we estimate the PER and also, as presented in next section, define the channel states based on the average SNR.

Here, we use the simulation results of the 90th percentile PER performance provided in the MB-OFDM proposal [12] and adopt the numerical method in [13] to obtain the closed-form approximation. The PER [12] of 110 Mbps MB-OFDM for 3a CM1 channels is plotted in Fig. 4. The observation suggests that we can split the PER curve into three segments, and each segment is fitted with an exponential curve (straight lines on the semi-log graph). Thus, the PER, ε, can be expressed as (with payload length of 1024 bytes):

$$\varepsilon(r') = 10^{a_i r' + b_i}, \tag{15}$$

where r' is the average received SNR. The coefficients, a_i and b_i, for each segment are obtained separately using linear regression and are listed in Table I. As shown in Fig. 4, the fitted curve is very close to the actual PER values.

[2]Due to the frequency-selective fading, the instantaneous received bit-energy and SNR of different subcarriers in MB-OFDM systems are random. The average received SNR, E_b/N_0, is defined as the ensemble average of SNR, which is determined by the transmitted power, path loss, implementation loss, antenna gain and shadowing.
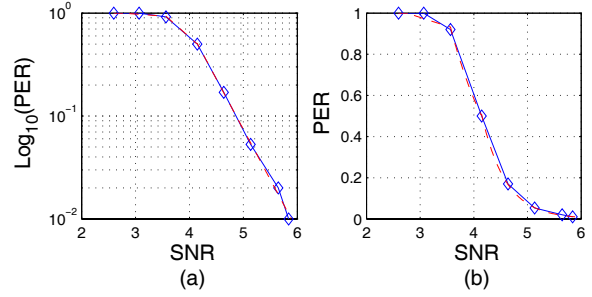

Fig. 4. PER for Mode 1 MB-OFDM systems in the CM1 channel environment ($-\diamond -$: simulation results[12]; $- -$: linear regression approximation).

TABLE I
COEFFICIENTS AND SPLITTING POINTS OF CURVE FITTING

Segments	SNR range (dB)	a_i	b_i
1	$0 \sim 3.56$	-0.0378	0.1041
2	$3.56 \sim 4.15$	-0.4657	1.6294
3	$4.15 \sim 5.84$	-0.9769	3.7547

The link budget analysis reveals the following observations. If the UWB transceivers are close enough or use low data rate transmission modes (TMs), the UWB system may have sufficient link margin to compensate for the additional channel loss caused by PSE. However, if the distance is large or high data rate TMs are employed, there is no sufficient link margin and the link performance will degrade significantly during people shadowing.

V. MARKOV MODEL FOR UWB CHANNEL WITH PEOPLE SHADOWING

In this section, we consider that a person randomly enters, moves around and exits the region between the UWB transceivers. Because the PER is dominated by the large-scale fading, we build a channel model based on the temporal fluctuation of the average SNR which is affected by the stochastic PSE. Then, the PER for each channel state is calculated given the obstructing positions and the received SNR.

A. Definition of Channel States

The average received SNR varies within a set range that depends on the position of the person. Fig. 5 shows the contour lines of the average received SNR. The x-axis and y-axis represent the obstructing position. The SNR values on the N contour lines are denoted as $R_n, n = 1, 2, \cdots, N$ and $R_{n+1} < R_n$. These contour lines divide the whole region into $N + 1$ zones. The zone between the two boundary contour lines of R_n and R_{n+1}, denoted as Z_n, corresponds to the SNR interval of $[R_{n+1}, R_n)$, which is defined as the nth channel state $S_n, n = 1, 2, \cdots, N-1$. The zone encompassed by the Nth contour line, denoted as Z_N, corresponds to the state S_N, which has the severest shadowing effect with the corresponding SNR interval $[R_{N+1}, R_N)$ where R_{N+1} is the minimum received SNR. In addition, we define state S_0 corresponding to the zone outside the most exterior contour line, Z_0, having the SNR interval $[R_1, R_0)$ where $R_0 = r(D)$
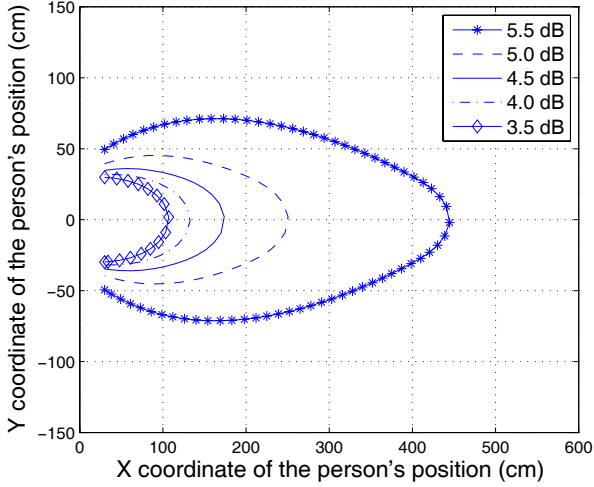
Fig. 5.   Average received SNR with shadowing effect.

TABLE II
PARAMETERS OF THE MARKOV MODEL

n	0	1	2	3	4	5
Area $A_n (m^2)$	-	2.978	0.773	0.323	0.172	0.357
λ_n ($/s$)	0.200	0.056	0.216	0.516	0.967	-
μ_n ($/s$)	-	0.112	0.431	1.032	1.934	1.400
p_n	0.324	0.578	0.075	0.016	0.004	0.003
PER $\bar{\varepsilon}_n$	0.006	0.039	0.128	0.392	0.764	0.987

is determined from (13). State S_0 represents when there is no person standing in the vicinity of the system.

Finally, the average PER of channel state S_n can be obtained as:

$$\bar{\varepsilon}_n = \begin{cases} \varepsilon\left[r\left(D\right)\right], & n = 0 \\ \frac{1}{A_n} \iint_{(x,y) \in Z_n} \varepsilon\left[r'\left(D, x, y\right)\right] dx dy, & n = 1, 2, \cdots, N \end{cases}$$

(16)

where the PER $\varepsilon(\cdot)$ is given by (15), the SNR $r(D)$ and $r'(D, x, y)$ are given by (13) and (14), respectively, and A_n is the area of the zone Z_n. Furthermore, the average throughput of state S_n can be approximated as:

$$\bar{H}_n = (1 - \bar{\varepsilon}_n)H, \quad n = 0, 1, \cdots, N$$

(17)

where H (Mbps) is the link throughput without packet error given in the MB-OFDM proposal [12].

Because the channel states correspond to the spatial zones and the person can only walk into adjacent zones from the current one, the shadowing process is a birth-death process with state transitions only to adjacent states. Thus, we construct a packet-level channel model using a first-order FSMC for the shadowed UWB channels.

B. State Transition Rate

The transition rates between the states are determined by the area of the zones and the person's mobility. Here, we assume a simple random walk model. The channel model can be extended to consider other mobility models such as those in [14], [15] for other specific scenarios.

First, the contour line of R_1 is the boundary of the shadowing region. An arriving person (entering the boundary) results in the onset of shadowing and the state transition from S_0 to S_1. We assume that the arrival of people is a Poisson process with the arrival rate λ_P, which increases with higher density and activity of the people inside the home or office. When the person moves out of the boundary, he (or another person) may re-enter the region later.

Second, because the instantaneous moving speed and direction of the person are varying randomly, the duration of

the person staying inside one zone is a random variable. We assume that the duration is exponentially distributed and the average duration is proportional to the area of the zone. Hence, the average duration of state S_n is $\bar{t}_n = A_n T$, where T is the average duration for which the person stays in a unit area. T is inversely proportional to the average movement speed. The departure rate from state S_n is $v_n = 1/\bar{t}_n = 1/(A_n T)$. Suppose that the probability of moving to the inner zone (from S_n to S_{n+1}) is α, $0 < \alpha < 1$. Thus, the transition rates to the adjacent inner zone are:

$$\lambda_n = \begin{cases} \lambda_P, & n = 0 \\ \alpha v_n = \frac{\alpha}{A_n T}, & n = 1, 2, \cdots, N - 1 \end{cases}$$

(18)

and the transition rates to the adjacent exterior zone (from S_n to S_{n-1}) are:

$$\mu_n = \begin{cases} (1 - \alpha)v_n = \frac{1-\alpha}{A_n T}, & n = 1, 2, \cdots, N - 1 \\ v_n = \frac{1}{A_n T}, & n = N. \end{cases}$$

C. Steady state probability

Denoting p_n as the steady-state probability of the channel state S_n, given the detailed equilibrium equations and the condition $\sum_{n=0}^{N} p_n = 1$, p_n can be derived as:

$$p_n = \begin{cases} \left[1 + \lambda_0 \sum_{i=1}^{N} \frac{1}{\mu_i} \left(\frac{\alpha}{1-\alpha}\right)^{i-1}\right]^{-1}, & n = 0 \\ \frac{\lambda_0}{\mu_n} \left(\frac{\alpha}{1-\alpha}\right)^{n-1} p_0, & n = 1, 2, \cdots, N \end{cases}$$

(19)

where λ_0 and μ_i are given in (18) and (19).

VI. NUMERICAL RESULTS

We evaluate the scenario that stationary UWB transceivers are deployed with a separation of $D = 15.5$ m. The data rate of the MB-OFDM system is 110 Mbps (according to the data rate versus range requirement of UWB systems). The payload size of a frame is 1024 bytes. The average received SNR is $r(D) = 6.16$ dB from (13) when there is no shadowing. The Markov model of $N = 6$ states is used here.

(1) Channel States

The contour lines of the average received SNR are plotted in Fig. 5. These five contour lines divide the region into six zones, which correspond to the six channel states as described in Section V-A. The SNR intervals for state S_0 to state S_5 are [5.5, 6.16), [5, 5.5), [4.5, 5), [4, 4.5), [3.5, 4) and [0, 3.5) dB, respectively. The average PER of each state is obtained from (16) and listed in Table II.

If single frame transmission mode is employed and there is no packet error, the throughput is $H = 83.48$ Mbps [12]. According to (17), the average throughput of each channel
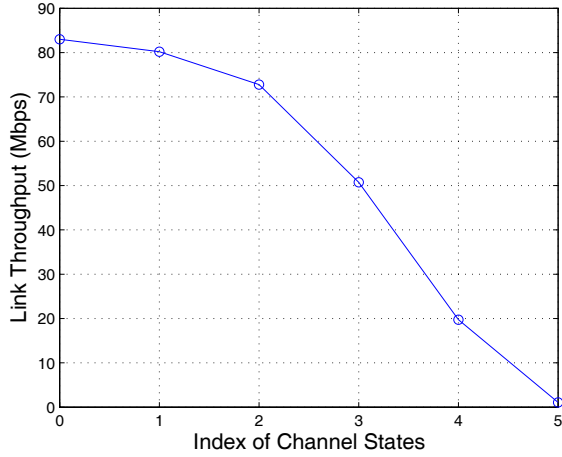
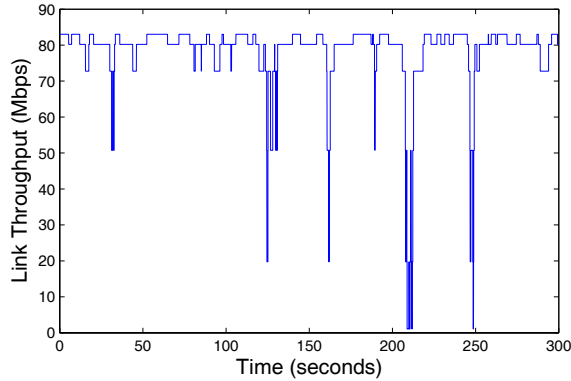Fig. 6.   Average throughput of the channel states.

Fig. 7.   Throughput fluctuation of a MB-OFDM link.

state is plotted in Fig. 6. It can be seen that the PER increases dramatically as the person gradually obstructs the main transmission paths, resulting in severely degraded link performance.

(2) Transition Rate

As an example of the people mobility model, we assume $\lambda_P = 0.2$ per second, $T = 2$ s/m^2 and $\alpha = 1/3$. The transition rate and steady state probabilities of the Markov channel model are obtained by (18), (19) and (19), respectively, and are listed in Table II. As expected, increasing λ_P leads to more frequent LOS shadowing and higher probability of changing shadowing states.

Fig. 7 illustrates the fluctuation of the throughput of the peer-to-peer MB-OFDM system. The channel temporal variation due to people interrupt is generated by the Markov model obtained above. Frequent fluctuation of the throughput from 80 Mbps to less than 20 Mbps can be observed, which can degrade the QoS of the on-going transmissions severely.

VII. CONCLUSIONS

In this paper, we have analyzed the PSE on indoor UWB channels. The power attenuation has been estimated based on the APSD and the position of obstruction. Furthermore, a packet-level channel model has been proposed for the

temporal variation of the UWB channels caused by the random movement of a person.

The proposed model is of high practical value as an analysis and simulation tool for UWB systems. Based on the channel model and the time-coherence property, we can optimize the channel estimation and power control mechanisms to improve the transmission efficiency. The model also promotes the research on the cross-layer designs. For example, the queuing behavior at link layer and the temporal variation of the realistic UWB channels can be analyzed and simulated jointly [16], which is important for improving QoS provisioning in WPANs.

APPENDIX A
DERIVATION OF EQ. (7)

From (5), we have:

$$\overline{\mathbb{P}(\theta)} = \sum_{k_0}^{\lfloor \tau_m \lambda \rfloor} E\left[\overline{P_{k,0}}\right] + \sum_{\lceil \tau_m \lambda \rceil}^{\infty} E\left[\overline{P_{k,0}}\right] + \sum_{l=1}^{\infty}\sum_{k=1}^{\infty} E\left[\overline{P_{k,l}}\right]$$

$$= \underbrace{\frac{\tau_m \Omega_0}{2\pi}\sum_{k_0}^{\lfloor \tau_m \lambda \rfloor} E\left[\frac{1}{t_{k,0}}e^{-\frac{t_{k,0}}{\gamma}}\right]}_{\bar{A}} + \underbrace{\frac{\Omega_0}{2\pi}\sum_{\lceil \tau_m \lambda \rceil}^{\infty} E\left[e^{-\frac{t_{k,0}}{\gamma}}\right]}_{\bar{B}}$$

$$+ \underbrace{\frac{\Omega_0}{2\pi}\sum_{l=1}^{\infty}\sum_{k=1}^{\infty} E\left[e^{-\frac{T_l}{\Gamma}}e^{-\frac{t_{k,l}}{\gamma}}\right]}_{\bar{C}}. \qquad (20)$$

Because $t_{k,0}$ has the distribution of $Gamma(k,\lambda)$, the probability density function is $f_{t_{k,0}}(x) = \frac{\lambda^k}{\Gamma(k)}x^{k-1}e^{-\lambda x}$ where $\Gamma(k) = (k-1)!$. The expectation in term $\bar{A}$ in (20) can be evaluated as:

$$E\left[\frac{1}{t_{k,0}}e^{-\frac{t_{k,0}}{\gamma}}\right] = \int_0^{\infty}\frac{1}{x}e^{-\frac{x}{\gamma}}\frac{\lambda^k}{\Gamma(k)}x^{k-1}e^{-\lambda x}dx$$

$$= \frac{\lambda^k}{\Gamma(k)}\int_0^{\infty}x^{k-2}e^{-(\frac{1}{\gamma}+\lambda)x}dx$$

$$= \frac{\lambda^k}{\Gamma(k)}\frac{(k-2)!}{(\frac{1}{\gamma}+\lambda)^{k-1}} = \frac{\lambda}{k-1}\rho^{k-1}, \quad (21)$$

where $\rho = \frac{\lambda\gamma}{1+\lambda\gamma}$. Because $k_0 \geq 2$ in (20), $k \geq 2$ and the convergence of the integral is guaranteed. Then, plug (21) into (20) and term $\bar{A}$ in (7) is obtained.

Similar to (21), we can obtain

$$E\left[e^{-\frac{t_{k,0}}{\gamma}}\right] = \int_0^{\infty}e^{-\frac{x}{\gamma}}\frac{\lambda^k}{\Gamma(k)}x^{k-1}e^{-\lambda x}dx$$

$$= \left(\frac{\lambda\gamma}{1+\lambda\gamma}\right)^k = \rho^k, \qquad (22)$$

where $k \geq 1$. Thus, term $\bar{B}$ in (20) can be obtained as

$$\bar{B} = \frac{\Omega_0}{2\pi}\sum_{\lceil \tau_m \lambda \rceil}^{\infty}\rho^k = \frac{\Omega_0}{2\pi}\frac{\rho^{\lceil \tau_m \lambda \rceil}}{1-\rho}. \qquad (23)$$

Because the random cluster delay T_l and ray delay $t_{k,l}$ are independent and have the distribution of $Gamma(l,\Lambda)$ and $Gamma(k,\lambda)$, respectively, using (22), term $\bar{C}$ in (20) is derived as:

$$\bar{C} = \frac{\Omega_0}{2\pi} \sum_{l=1}^{\infty} \sum_{k=1}^{\infty} E\left[e^{-\frac{T_l}{\Gamma}}\right] E\left[e^{-\frac{t_{k,l}}{\gamma}}\right]$$

$$= \frac{\Omega_0}{2\pi} \sum_{l=1}^{\infty} \sum_{k=1}^{\infty} \left(\frac{\Gamma\Lambda}{1+\Gamma\Lambda}\right)^l \left(\frac{\lambda\gamma}{1+\lambda\gamma}\right)^k$$

$$= \frac{\Omega_0}{2\pi} \sum_{l=1}^{\infty} \left(\frac{\Gamma\Lambda}{1+\Gamma\Lambda}\right)^l \sum_{k=1}^{\infty} \left(\frac{\lambda\gamma}{1+\lambda\gamma}\right)^k$$

$$= \frac{\Omega_0}{2\pi}(\Gamma\Lambda)(\gamma\lambda). \tag{24}$$

Combining (21), (23) and (24) gives (7).

APPENDIX B
DERIVATION OF EQ.(8)

The average power of each ray conditioned on the cluster delay and ray delay is given in (2). The delay for the first cluster is $T_0 = 0$. Using (22), the expectation of the total power of the CIR can be evaluated as:

$$E_t = E\left[\sum_{l=0}^{\infty} \sum_{k=1}^{\infty} E[|a_{k,l}|^2]\right] = \Omega_0 \sum_{l=0}^{\infty} \sum_{k=1}^{\infty} E\left[e^{-\frac{T_l}{\Gamma}} e^{-\frac{t_{k,l}}{\gamma}}\right]$$

$$= \Omega_0 \sum_{l=0}^{\infty} \left(\frac{\Gamma\Lambda}{1+\Gamma\Lambda}\right)^l \sum_{k=1}^{\infty} \left(\frac{\lambda\gamma}{1+\lambda\gamma}\right)^k$$

$$= \Omega_0(1+\Gamma\Lambda)(\gamma\lambda). \tag{25}$$

Here, $E\left[e^{-\frac{T_0}{\Gamma}}\right] = 1 = \left(\frac{\Gamma\Lambda}{1+\Gamma\Lambda}\right)^0$. To normalize the total power of the multipath components, set $E_t = 1$ and we obtain (8).

REFERENCES

[1] W. Zhuang, X. Shen, and Q. Bi, "Ultra-wideband wireless communications," *Proc. Wireless Commun. Mobile Computing (WCMC)/Wiley*, vol. 3, no. 6, pp. 663-685, 2003.

[2] P. Pagani and P. Pajusco, "Characterization and modeling of temporal variations on an ultrawideband radio link," *IEEE Trans. Antennas Propag.*, vol. 54, no. 11, pp. 3198-3206, Nov. 2006.

[3] ——, "Experimental assessment of the UWB channel variability in a dynamic environment," in *Proc. IEEE Int. Symp. Personal, Indoor Mobile Radio Commun.*, vol. 4, Barcelona, Spain, Sept. 2004, pp. 2973-2977.

[4] Z. Irahhauten, J. Dacuna, G. J. Janssen, and H. Nikookar, "UWB channel measurements and results for wireless personal area networks applications," in *Proc. European Conf. Wireless Technology*, Paris, France, Oct. 2005, pp. 189-192.

[5] S. V. Schell, "Analysis of time variance of a UWB propagation channel," IEEE P802.15-02/452r0-SG3a, Tech. Rep., Nov. 2002.

[6] M. Ghaddar, L. Talbi, and T. Denidni, "A conducting cylinder for modeling human body presence in indoor propagation channel," *IEEE Trans. Antennas Propag.*, vol. 55, no. 11, pp. 3099-3103, 2007.

[7] J. Foerster *et al.*, "Channel modeling sub-committee report final," IEEE 802.15-02/490, Tech. Rep., Feb. 2003.

[8] R. Zhang and L. Cai, "A Markov model for indoor ultra-wideband channel with people shadowing," *ACM/Springer Mobile Networks and Applications (MONET)*, special issues on mobility of systems, users, data and computing, vol. 12, no. 5-6, pp. 438-449, Dec. 2007.

[9] Q. Spence, B. Jeffs, M. Jensen, and A. Swindlehurst, "Modeling the statistical time and angle of arrival characteristics of an indoor multipath channel," *IEEE J. Select. Areas Commun.*, vol. 18, no. 3, pp. 347-360, Mar. 2000.

[10] R. Cramer, R. Scholtz, and M. Win, "Evaluation of an ultra-wide-band propagation channel," *IEEE Trans. Antennas Propag.*, vol. 50, no. 5, pp. 561-570, May 2002.

[11] A. Molisch, "Time variance for UWB wireless channels," IEEE P802.15-02/461r0, Tech. Rep., Nov. 2002.

[12] *Multi-band OFDM Physical Layer Proposal for IEEE 802.15 Task Group 3a*, IEEE P802.15.3a Working Group, P802.15-03/268r3, Mar. 2004.

[13] G. T. Nguyen, R. H. Katz, B. Noble, and M. Satyanarayanan, "A trace-based approach for modeling wireless channel behavior," in *Proc. 28th Conf. Winter Simulation*, Coronado, CA, USA, 1996, pp. 597-604.

[14] J. Yoon, M. Liu, and B. Noble, "Random waypoint considered harmful," in *Proc. INFOCOM'03*, San Francisco, CA, USA, Apr. 2003.

[15] G. Lin, G. Noubir, and R. Rajamaran, "Mobility models for ad-hoc network simulation," in *Proc. INFOCOM'04*, Hong Kong, China, Mar. 2004.

[16] K. Liu, X. Shen, R. Zhang, and L. Cai, "Performance analysis of distributed reservation protocol for UWB-based WPAN," *IEEE Trans. Veh. Technol.*, vol. 58, no. 2, pp. 902-913, Feb. 2009.

Ruonan Zhang received the B.S. and M.S. degrees in electrical engineering from Xi'an Jiaotong University, Shaanxi Province, China, in 2000 and 2003, respectively. He was with Motorola Inc. and later with Freescale Semiconductor Inc. in Tianjin, China, from 2003 to 2006, working on IC architecture and application design. He is now working toward the Ph.D. degree at the Department of Electrical and Computer Engineering, University of Victoria, British Columbia, Canada. His current research interests include cross-layer design and optimization for wireless networks and wireless personal area network (WPAN).

Lin Cai (S'00-M'06) received the M.A.Sc. and Ph.D. degrees (with Outstanding Achievement in Graduate Studies Award) in electrical and computer engineering from the University of Waterloo, Waterloo, Canada, in 2002 and 2005, respectively. Since July 2005, she has been an Assistant Professor in the Department of Electrical and Computer Engineering at the University of Victoria, British Columbia, Canada. Her research interests span several areas in wireless communications and networking, with a focus on network protocol and architecture design supporting emerging multimedia traffic over wireless, mobile, ad hoc, and sensor networks. She serves as the Associate Editor for IEEE TRANSACTIONS ON VEHICULAR TECHNOLOGY (2007-), EURASIP JOURNAL ON WIRELESS COMMUNICATIONS AND NETWORKING (2006-), and INTERNATIONAL JOURNAL OF SENSOR NETWORKS (2006-).